Implications of Dedicated Seismometer Measurements on Newtonian-Noise Cancellation for Advanced LIGO

M. W. Coughlin, J. Harms, J. Driggers, D. J. McManus, N. Mukund, M. P. Ross, B. J. J. Slagmolen, and K. Venkateswara

Phys. Rev. Lett. **121**, 221104 — Published 28 November 2018

DOI: 10.1103/PhysRevLett.121.221104

Implications of dedicated seismometer measurements on Newtonian-noise cancellation for Advanced LIGO

M. W. Coughlin,[1] J. Harms,[2,3] J. Driggers,[4] D. J. McManus,[5] N. Mukund,[6] M. P. Ross,[7] B. J. J. Slagmolen,[5] and K. Venkateswara[7]

[1]*Division of Physics, Math, and Astronomy, California Institute of Technology, Pasadena, CA 91125, USA*
[2]*Gran Sasso Science Institute (GSSI), I-67100 LAquila, Italy*
[3]*INFN, Laboratori Nazionali del Gran Sasso, I-67100 Assergi, Italy*
[4]*LIGO Hanford Observatory, Richland, WA, 99352, USA*
[5]*OzGrav, Australian National University, Research School of Physics and Engineering, Canberra, Australian Capital Territory 2601, Australia*
[6]*Inter-University Centre for Astronomy and Astrophysics (IUCAA), Post Bag 4, Ganeshkhind, Pune 411 007, India*
[7]*Department of Physics, University of Washington, Seattle, WA 98195, USA*

Newtonian gravitational noise from seismic fields will become a limiting noise source at low frequency for second-generation, gravitational-wave detectors. It is planned to use seismic sensors surrounding the detectors' test masses to coherently subtract Newtonian noise using Wiener filters derived from the correlations between the sensors and detector data. In this work, we use data from a seismometer array deployed at the corner station of the LIGO Hanford detector combined with a tiltmeter for a detailed characterization of the seismic field and to predict achievable Newtonian-noise subtraction levels. As was shown previously, cancellation of the tiltmeter signal using seismometer data serves as the best available proxy of Newtonian-noise cancellation. According to our results, a relatively small number of seismometers is likely sufficient to perform the noise cancellation due to an almost ideal two-point spatial correlation of seismic surface displacement at the corner station, or alternatively, a tiltmeter deployed under each of the two test masses of the corner station at Hanford will be able to efficiently cancel Newtonian noise. Furthermore, we show that the ground tilt to differential arm-length coupling observed during LIGO's second science run is consistent with gravitational coupling.

PACS numbers: 95.75.-z,04.30.-w

Detections of gravitational waves (GWs) by the Advanced LIGO [1] and Virgo [2] detectors from compact binaries such as binary black holes [3–6] and binary neutron stars [7] can be facilitated by improving low-frequency sensitivity of GW detectors. In particular, detection of higher mass mergers (and at higher rates) is possible as the low-frequency sensitivity improves [8]. In addition, increasing sensitivity at low frequencies can significantly improve our ability to estimate certain signal parameters such as the individual masses of the two compact objects and lead to more stringent tests of general relativity [8–11].

One of the major noise contributions below 30 Hz comes from terrestrial gravity fluctuations, also known as Newtonian noise (NN) [12, 13]. These gravity fluctuations are predominantly from two sources: density perturbations in the atmosphere, or from seismic fields. Seismic surface fields are predicted to dominate the NN contribution [14], although recent measurements at Virgo show that the atmosphere can be important as well [15]. While the average NN is likely to lie below the instrumental noise of the Advanced LIGO and Virgo detectors, at times of higher environmental noise, it can dominate [14].

It was proposed to mitigate NN by monitoring the environmental fields with sensor arrays [16]. Since site-characterization measurements suggest that seismic fields at the LIGO sites are dominated by surface Rayleigh waves in the LIGO NN band between 10 Hz and 20 Hz from local sources [17], NN mitigation can be achieved by deploying a surface array around each test mass monitoring vertical ground displacements [14].

The conventional approach of NN subtraction is to create Wiener filters using data from sensor arrays, similar to feed-forward cancellation schemes already used with other detector noise [18–20]. Previous work was concerned with optimizing the placement of seismometers using high-dimensional samplers minimizing the expected noise residuals [14, 17]. Wiener filters are typically constructed using observed correlations between sensors, although models of the seismic field can be employed as well [17]. Harms and Venkateswara [21] also showed that a single seismic tiltmeter can be used to strongly reduce NN only limited by tiltmeter self-noise, provided that the seismic field is accurately represented by plane-wave models. However, since we do not have a quantitative measure yet what "accurate" means, it is impossible right now to guarantee that a tiltmeter will be sufficient no matter how weakly observations deviate from a plane-wave model.

In this Letter, we present first results of the cancellation of a tilt signal in the frequency range 10 Hz — 20 Hz measured by a compact beam-rotation sensor [21], and give a detailed characterization of the seismic field for the purpose of NN cancellation. We first show that the seis-

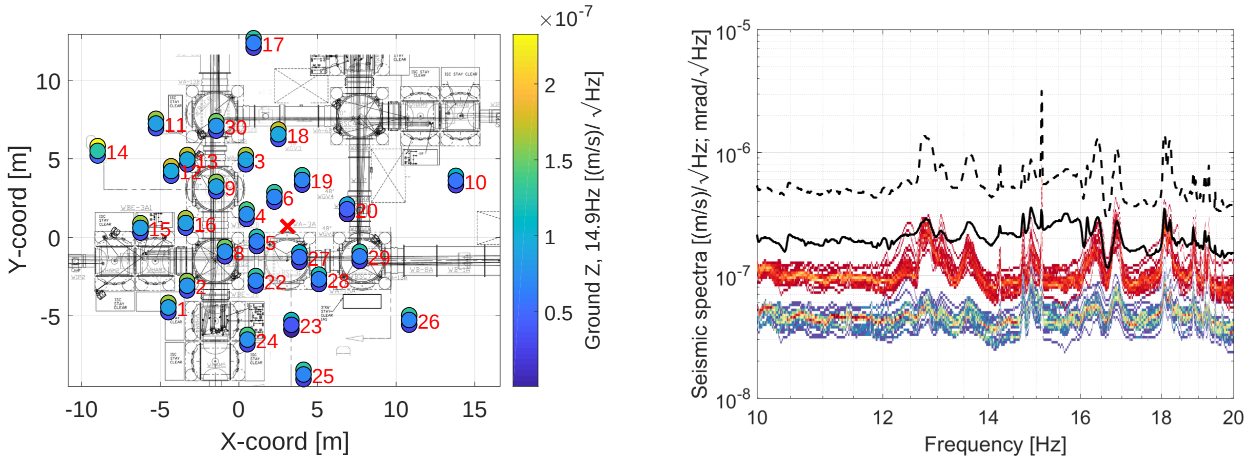

FIG. 1: On the left is the layout of the instrument floor at the corner station of the LIGO Hanford Observatory, with the location of the L-4C's indicated by the coloured circles and its number. For each seismometer, the 10th, 50th, and 90th percentiles of the square-root of power spectral densities (PSDs) at 15 Hz are indicated from bottom to top with the colored circles. The red cross marks the location of the tiltmeter during the first months of the O2 science run. On the right are histograms of the 50th and 90th percentiles of seismic spectra collected from all seismometers in units $(\mathrm{m/s})/\mathrm{Hz}^{-1/2}$. The black lines are the 50th (solid) and 90th (dashed) percentiles of the tiltmeter spectra in units $\mathrm{mrad}/\mathrm{Hz}^{-1/2}$.

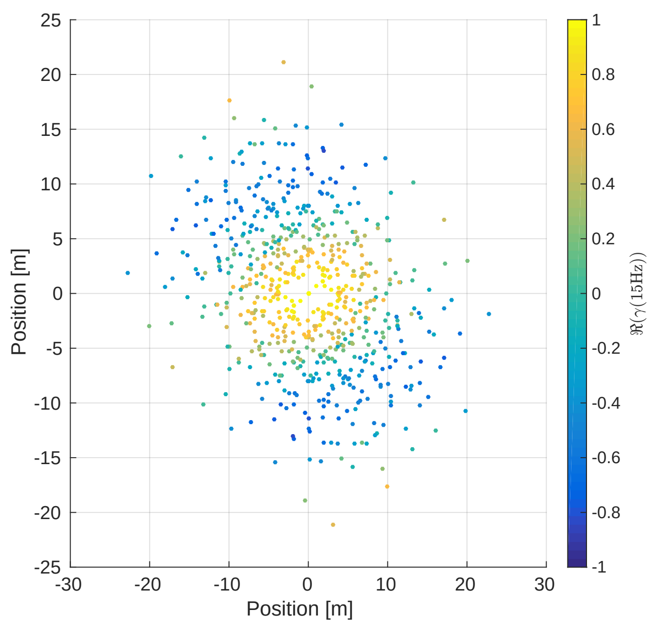

FIG. 2: The measured correlation function for the LIGO Hanford corner station at 15 Hz.

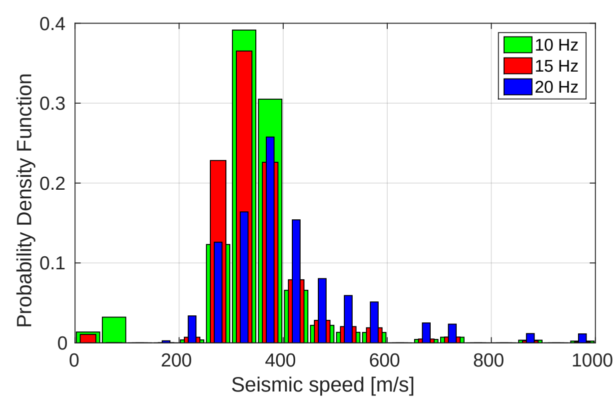

FIG. 3: Histograms of seismic speed measurements using LHO array data at 10 Hz, 15 Hz, and 20 Hz.

mic field is approximately homogeneous and dominated by Rayleigh waves, which is important as seismic fields with a mixture of wave types would be very difficult for any NN subtraction [13]. We then implement an optimal subtraction scheme using the array of seismometers as input to a Wiener filter and the tiltmeter as target channel. The investigation with the tiltmeter as a target channel is important, because ground tilt along the direction of the detector arm is fully coherent with NN from plane Rayleigh waves, and therefore is the best available proxy for testing NN cancellation schemes [13].

Beginning of October 2016, an array of 30 L-4C vertical-axis seismometers [24] were deployed at the corner station building at LIGO Hanford. Concurrently, a single-axis tiltmeter was installed at the center of the array [21, 22]. The left of Figure 1 shows the locations of the seismometers in the vicinity of the vacuum enclosure. The data from the seismometers are conditioned, acquired digitally and saved at a 512 Hz sampling rate. The configuration of seismometers was an approximately equidistant placement of a few meters between neighbors in the central part of the array and increased spacing along the edges. For the analysis, we divide the time-series data into 50% overlapping 128 s segments that are Hann-windowed. The first metric presented are percentiles of the PSDs, which show variations in the seismic field over the frequency band of interest. Each sensor in the map of Figure 1 is represented by 3 overlaid circles, the lower one representing the 10th percentile at 15 Hz, the middle one the 50th, and the upper one the 90th percentile. Maps at other frequencies can be found in the Supplement. These maps allow us to identify local sources, or locations of vibration amplification due to interaction with infrastructure. The plot on the right shows the full spectra of all sensors for the 50th and 90th percentiles. The spectra have significant structure over the 10-20 Hz band indicating the presence of several relatively narrow-band local sources.

The second metric presented is the complex coherence, $\gamma(f)$, between the seismometers in the array, calculated as $\gamma(f) = \frac{\langle x(f)\, y^*(f)\rangle}{\sqrt{\langle |x(f)|^2\rangle \langle |y(f)|^2\rangle}}$ where $x(f)$ and $y(f)$ are the values of the Fourier Transform at a particular frequency f for two seismometers. This quantity allows for the characterization of the seismic field and is also an important quantity for the calculation of noise-cancellation filters [16, 17]. Figure 2 shows a measurement of $\Re(\gamma)$ between all 27 seismometers used for this study at 15 Hz. Each coherence value is drawn at a coordinate, which corresponds to the relative position vector between the two sensors. Although there are some instances of inhomogeneities where high coherence points are near to low coherence points, in general the coherence evolves smoothly, and consistently with a Rayleigh-wave field. Homogeneity is a prerequisite for realizing NN cancellation with a relatively small number of seismometers (not more than 10 seismometers per test mass). The Supplement explores the variability in this quantity. Accounting for inhomogeneity is currently an open problem, and a much denser spatial sampling of the seismic field might be required to predict its effect on NN cancellation [17].

The third metric presented is a measurement of wave speeds in the frequency range 10 Hz – 20 Hz shown in Figure 3, which is useful for further characterization of the field and predictions of the levels of Wiener filter subtraction that could be expected. We used the method of section 3.6.3 of [13]. The idea is to decompose the seismic field into plane harmonics and collect the phase speeds associated with the maximum-amplitude component. Consistent with measurements at the end stations [17], the average velocities are about 300 m/s at 10 Hz and 15 Hz and 380 m/s at 20 Hz, which is thought to be due to the concrete slab of the laboratory building, which has greater effect at shorter seismic wavelengths. Outliers in the histogram might be from body waves at higher speeds, or simply be the result of aliasing effects, which can happen when several waves at the same frequency simultaneously propagate through the array. Otherwise, these measurements are consistent with Rayleigh waves, which simplifies the NN modeling [13]. The width of the distribution can be explained by broadening due to sources being relatively close to the array giving rise to circular wave fronts, due to anisotropy of the ground, and potentially also due to seismic scattering (the latter two are likely minor effects at the LIGO sites since the soil does not vary significantly in horizontal directions over the extent of the array, and the surface is flat).

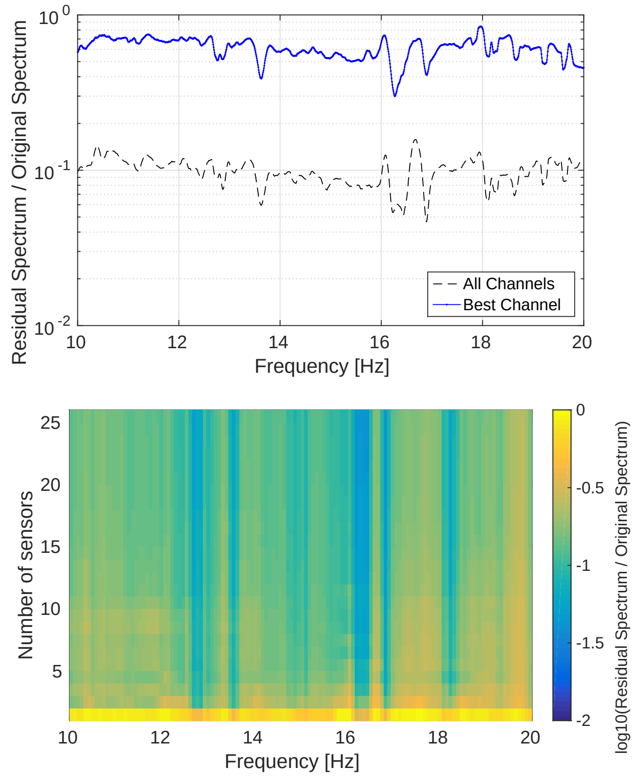

FIG. 4: Top panel: spectrum of average subtraction residuals $\sqrt{R}$ in the tiltmeter calculated from Equation (1) using all available seismometers as witnesses or the single most effective seismometer picked for each frequency. Bottom panel: average residuals in the tiltmeter for all possible numbers of seismometers picked from the array such that residuals at 15 Hz are minimized.

As discussed above, Wiener filters use correlations between reference data streams and a target data stream to give an estimate of the noise contributions to the target sensor present in the reference data streams as well [23]. In the regime where all data streams have stationary noise, they are known to be optimal filters. In this work, we take a tiltmeter as our target sensor, with seismometers as reference data streams.

In the following, we will denote the cross-spectral densities between the N seismometers in the array as $C_{\rm SS}(f)$, which is a $N \times N$ matrix. Similarly, we take the cross-spectral density between array and tiltmeter, which has N terms, as $\vec{C}_{\rm ST}(f)$. We finally denote the PSD of the target sensor as $C_{\rm TT}(f)$. The Wiener filter is then constructed as $\vec{w}(f) = \vec{C}_{\rm ST}^{\top}(f) \cdot C_{\rm SS}^{-1}(f)$, where $C_{\rm ST}^{\top}(f)$ is the transpose of $\vec{C}_{\rm ST}(f)$ and $C_{\rm SS}^{-1}(f)$ is the inverse matrix of $C_{\rm SS}(f)$. The estimate of the target sensor data is then simply $\vec{w}(f)\cdot\vec{s}(f)$, where $\vec{s}(f)$ are the Fourier transforms at frequency f of segments of data from all seismometers. Note that a similar definition of the Wiener filter can be given in time domain, realized for example as finite impulse-response filter.

We can use the coherence results to determine the average residuals. Based on the above quantities, the average relative noise residual R is determined by

$$R = 1 - \frac{\vec{C}_{\rm ST}^{\top}\cdot C_{\rm SS}^{-1}\cdot \vec{C}_{\rm ST}}{C_{\rm TT}}. \tag{1}$$

In Figure 4, we use Equation (1) to determine average residuals. To determine the optimal configurations used for the bottom plot, we simply loop over all configurations for a given number of seismometers picked from the entire array and identify the one with the smallest residual at 15 Hz . Based upon this, the average residuals rapidly converge after only a few seismometers. We note that this is a different method than in Coughlin et al. [17] where the sensor locations were allowed to vary arbitrarily and correlations were based on a model fit to the observed correlations. We show representative optimal array configurations in the Supplement. Based upon this, we expect significant suppression of tilt signals. We also find that it is unlikely to be necessary to update the Wiener filters often, since subtraction performance did not change significantly over the course of months (see supplement), which means that the Wiener filter cab be implemented as static filter.

The Wiener filter can be studied further by calculating its Bode plot shown in Figure 5, which consists of the magnitude and phase of the filter for each witness channel as a function of frequency. The plots show that some seismometers form tiltmeter type configurations. These can be identified by searching for pairs of seismometers whose magnitudes are similar over the entire frequency band, and with a relative phase of about 180°. Sensors 4, 5, 20, and 27 form two such pairs. Many sensors contribute to the Wiener filter with similar magnitude. Combined with the observation from Figure 4 that around 5 sensors or less are required to achieve most of the noise cancellation, similar magnitudes of sensors in a larger array means that the main impact of additional sensors is to average incoherent noise. We cannot fully explain the low magnitude of sensor 14 over the entire band. As the PSD maps indicate, see Figure 1 and supplement, the seismic signal at many frequencies is much stronger at sensor 14 than at other sensors used in Figure 5. This would explain the relatively low magnitude. However, its signal is weaker closer to 20 Hz than in other sensors. This begs the question why the magnitude does not rise towards higher frequencies. It might be that its signal at higher frequencies is actually below its instrumental noise so that the Wiener filter suppresses injection of incoherent noise into the target channel. This hypothesis does not seem to be consistent though with such low magnitude values. It will be very important to study Bode plots of Wiener filters in greater detail to obtain an intuitive understanding of how the filter retrieves information from the witness channels, which could guide optimal placement of sensors even in inhomogeneous seismic fields where numerical methods still fail.

Last, we present measurements of transfer functions between ground tilt and GW data 'h(t)' shown in Figure 6. Newtonian noise is predicted to lie about a factor 100 below other instrumental noise during the second science run, so that long correlation times need to be used to observe gravitational coupling. Our measurements use about 1 month of data with the interferometer locked starting in December 2016. A NN model is plotted for an isotropic, homogeneous field taking into account that seismic waves generally produce NN through both test masses of the corner station, and considering the positions of the two test masses and tiltmeter. The direct measurement of the transfer function from ground tilt to h(t) is shown as blue, solid line. Additional couplings were investigated through the seismic isolation system: displacement of the test-mass suspension-point along the arm (Sus L), and pitch, i.e., a rotation around the horizontal axis perpendicular to the arm, of the suspension table (Sus P). The measured transfer function from ground tilt to Sus L can be subsequently passed through a model of the quadruple suspension system (solid, violet line), or through a measured transfer function between Sus L and h(t) (solid, yellow line). The yellow line corresponds in fact to the sum of the two transfer functions through Sus L and P (which does not accurately represent the total coupling through Sus L/P since it ignores correlations between these two channels). Last, the measurement noise is shown, which was calculated by sliding the ground tilt and h(t) time series against each other by about 1000 s, and also by an analytic Gaussian model of measurement noise (which both give almost identical curves).

With the exception of a few frequencies, the observed ground tilt to h(t) coupling (solid, blue) lies well above the measurement noise (dot-dashed, black) up to about 20 Hz. It is inconsistent with contributions from suspension point motion, which by itself is inconsistent with a model of mechanical coupling through the suspension stages (hinting towards additional coupling mechanisms). The observed ground tilt to h(t) coupling is consistent with a simple (isotropic, homogeneous) NN model above about 13 Hz where deviations between observation and model are small enough to be explained by the weak anisotropies (and potentially inhomogeneities) of the seismic field visible in Figure 2.

In summary, we have used dedicated measurements at the LIGO Hanford site to predict NN cancellation levels.

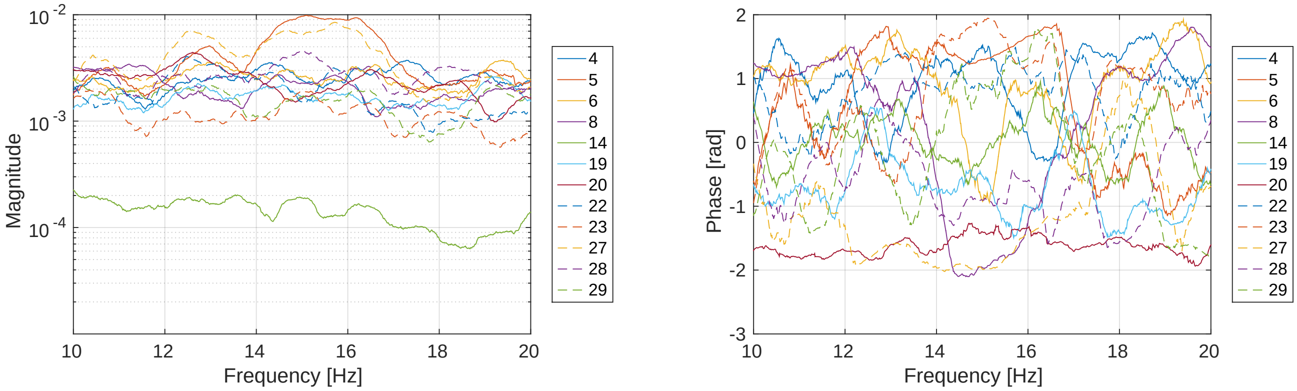

FIG. 5: The magnitude (left) and phase (right) of the Wiener filter using 12 optimally picked witness channels.

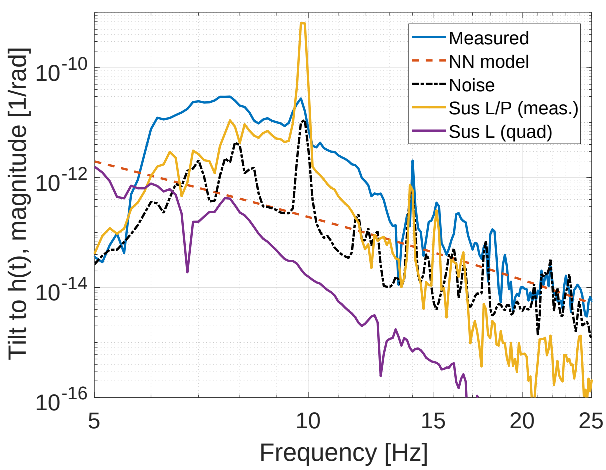

FIG. 6: Ground tilt to GW data couplings.

We achieved suppression of a tiltmeter signal by a factor of about 10 throughout the NN band using data from a seismometer array serving as a proxy for NN cancellation in a GW detector. The near-ideal form of the two-point spatial correlations together with the cancellation results suggests that NN cancellation with few seismometers or a tiltmeter at each test mass will be feasible. We further provided strong constraints on the NN spectrum by analyzing correlations between the tiltmeter and GW data, which allow us to conclude that it is highly unlikely that NN will be significantly stronger than predicted in the past. The result also shows that there is significant noise in the detector data that we will be able to subtract with a tiltmeter independent of the coupling mechanism.

MC was supported by the David and Ellen Lee Postdoctoral Fellowship at the California Institute of Technology. NM acknowledges Council of Scientific and Industrial Research (CSIR), India for providing financial support as Senior Research Fellow. BS was supported by ARC Future Fellowship FT130100329 and DM and BS are supported by the ARC Centre of Excellence for Gravitational Wave Discovery. Thanks to the Seismic Working Group of the LIGO Scientific Collaboration for the suspension model. LIGO was constructed by the California Institute of Technology and Massachusetts Institute of Technology with funding from the National Science Foundation and operates under cooperative agreement PHY-0757058. The authors thank the LIGO Scientific Collaboration for access to the data and gratefully acknowledge the support of the United States National Science Foundation (NSF) for the construction and operation of the LIGO Laboratory and Advanced LIGO as well as the Science and Technology Facilities Council (STFC) of the United Kingdom, and the Max-Planck-Society (MPS) for support of the construction of Advanced LIGO. Additional support for Advanced LIGO was provided by the Australian Research Council. This paper has been assigned LIGO document number LIGO-P1800049.

References

[1] J Aasi et al 2015 *Classical and Quantum Gravity* **32** 074001 URL `http://stacks.iop.org/0264-9381/32/i=7/a=074001`

[2] F Acernese et al 2015 *Classical and Quantum Gravity* **32** 024001 URL `http://stacks.iop.org/0264-9381/32/i=2/a=024001`

[3] Abbott, B P et al (LIGO Scientific Collaboration and Virgo Collaboration) 2016 *Phys. Rev. Lett.* **116**(6) 061102 URL `http://link.aps.org/doi/10.1103/PhysRevLett.116.061102`

[4] Abbott, B P et al (LIGO Scientific Collaboration and Virgo Collaboration) 2016 *Phys. Rev. Lett.* **116**(24) 241103 URL `http://link.aps.org/doi/10.1103/PhysRevLett.116.241103`

[5] Abbott, B P et al (LIGO Scientific and Virgo Collaboration) 2017 *Phys. Rev. Lett.* **118**(22) 221101 URL https://link.aps.org/doi/10.1103/PhysRevLett.118.221101
[6] Abbott, B P et al (LIGO Scientific Collaboration and Virgo Collaboration) 2017 *Phys. Rev. Lett.* **119**(14) 141101 URL https://link.aps.org/doi/10.1103/PhysRevLett.119.141101
[7] Abbott, B P et al (LIGO Scientific Collaboration and Virgo Collaboration) 2017 *Phys. Rev. Lett.* **119**(16) 161101 URL https://link.aps.org/doi/10.1103/PhysRevLett.119.161101
[8] Yu H, Martynov D, Vitale S, Evans M, Shoemaker D, Barr B, Hammond G, Hild S, Hough J, Huttner S, Rowan S, Sorazu B, Carbone L, Freise A, Mow-Lowry C, Dooley K L, Fulda P, Grote H and Sigg D 2018 *Phys. Rev. Lett.* **120**(14) 141102 URL https://link.aps.org/doi/10.1103/PhysRevLett.120.141102
[9] B Sathyaprakash et al 2012 *Classical and Quantum Gravity* **29** 124013 URL http://stacks.iop.org/0264-9381/29/i=12/a=124013
[10] Lynch R, Vitale S, Barsotti L, Dwyer S and Evans M 2015 *Phys. Rev. D* **91**(4) 044032 URL http://link.aps.org/doi/10.1103/PhysRevD.91.044032
[11] Harry I and Hinderer T 2018 *Classical and Quantum Gravity* **35** 145010 URL http://stacks.iop.org/0264-9381/35/i=14/a=145010
[12] Saulson P R 1984 *Phys. Rev. D* **30**(4) 732–736 URL http://link.aps.org/doi/10.1103/PhysRevD.30.732
[13] Harms J 2015 *Living Reviews in Relativity* **18** URL http://www.livingreviews.org/lrr-2015-3
[14] Driggers J C, Harms J and Adhikari R X 2012 *Phys. Rev. D* **86**(10) 102001 URL http://link.aps.org/doi/10.1103/PhysRevD.86.102001
[15] Fiorucci D, Harms J, Barsuglia M, Fiori I and Paoletti F 2018 *Phys. Rev. D* **97**(6) 062003 URL https://link.aps.org/doi/10.1103/PhysRevD.97.062003
[16] Cella G 2000 Off-line Subtraction of Seismic Newtonian Noise *Recent Developments in General Relativity* (Springer) pp 495–503
[17] Coughlin M, Mukund N, Harms J, Driggers J, Adhikari R and Mitra S 2016 *Classical and Quantum Gravity* **33** 244001 URL http://stacks.iop.org/0264-9381/33/i=24/a=244001
[18] Giaime J A, Daw E J, Weitz M, Adhikari R, Fritschel P, Abbott R, Bork R and Heefner J 2003 *Review of Scientific Instruments* **74** 218–224 URL http://scitation.aip.org/content/aip/journal/rsi/74/1/10.1063/1.1524717
[19] Driggers J C, Evans M, Pepper K and Adhikari R 2012 *Review of Scientific Instruments* **83** 024501–024501–6 ISSN 0034-6748
[20] DeRosa R, Driggers J C, Atkinson D, Miao H, Frolov V, Landry M, Giaime J A and Adhikari R X 2012 *Classical and Quantum Gravity* **29** 215008 URL http://stacks.iop.org/0264-9381/29/i=21/a=215008
[21] Harms J and Venkateswara K 2016 *Classical and Quantum Gravity* **33** 234001 URL http://stacks.iop.org/0264-9381/33/i=23/a=234001
[22] Venkateswara K, Hagedorn C A, Turner M D, Arp T and Gundlach J H 2014 *Review of Scientific Instruments* **85** 015005 URL http://scitation.aip.org/content/aip/journal/rsi/85/1/10.1063/1.4862816
[23] Benesty J, Huang Y and Chen J 2008 Wiener and Adaptive Filters *Springer Handbook of Speech Processing* ed Benesty J, Sondhi M and Huang Y (Springer Berlin Heidelberg) pp 103–120 ISBN 978-3-540-49125-5 URL http://dx.doi.org/10.1007/978-3-540-49127-9_6
[24] www.sercel.com/products/Pages/seismometers.aspx